Environmental Science Processes & Impacts

PAPER

View Article Online
View Journal | View Issue

Cite this: *Environ. Sci.: Processes Impacts*, 2019, **21**, 748

Effects of vertical hydrodynamic mixing on photomineralization of dissolved organic carbon in arctic surface waters†

Angang Li,[a] Antoine F. Aubeneau,*[b] Tyler King,[c] Rose M. Cory,[d] Bethany T. Neilson,[c] Diogo Bolster[e] and Aaron I. Packman[a]

Received 2nd October 2018
Accepted 8th March 2019

DOI: 10.1039/c8em00455b

rsc.li/espi

Photomineralization, the transformation of dissolved organic carbon (DOC) to CO_2 by sunlight, is an important source of CO_2 in arctic surface waters. However, quantifying the role of photomineralization in inland waters is limited by the understanding of hydrologic controls on this process. To bridge this gap, this study evaluates mixing limitations, *i.e.*, whether and by how much vertical mixing limits the depth-integrated photomineralization rate, in freshwater systems. We developed a conceptual model to qualitatively assess mixing limitations across the range of light attenuation and hydrologic conditions observed in freshwaters. For the common case of exponential light attenuation over depth, we developed a mathematical model to quantify mixing limitation, and used this model to assess a range of arctic freshwater systems. The results demonstrate that mixing limitations are important when there is significant light attenuation by suspended sediment (SS), which is the case in some arctic, boreal and temperate waters. Mixing limitation is pronounced when light attenuation over depth is strong and when the photomineralization rate at the water surface exceeds the vertical mixing rate. Arctic streams and rivers have strong vertical mixing relative to surface photomineralization, such that model results demonstrate no mixing limitation regardless of how much SS is present. Our analysis indicates that well-mixed assumptions used in prior work are valid in many, but not all, arctic surface waters. The effects of mixing limitations in reducing the photomineralization rate must be considered in arctic lakes with high SS concentrations.

Environmental significance

Dissolved organic carbon (DOC), found in all waters on Earth, is converted to CO_2, a greenhouse gas, upon exposure to sunlight in surface waters. Greenhouse gas emissions from arctic surface waters are important components of the global carbon cycle now and in the future as the Arctic warms and permafrost soils thaw. Arctic permafrost thaw will expose a substantial amount of dissolved organic carbon (DOC) to sunlight. Currently, sunlight-driven conversion of DOC to CO_2 accounts for about one third of the CO_2 released from Alaskan arctic surface waters. However, how this may change in the future is not well known due to knowledge gaps on the underlying hydrologic controls on sunlight-driven (photochemical) conversion of DOC to CO_2. Our study is the first attempt to quantify the effect of vertical water-column mixing on rates of DOC photochemical conversion to CO_2. We present and develop both conceptual and numerical models to assess the importance of vertical mixing on rates of DOC photochemical conversion to CO_2 in arctic freshwaters. Our results show the importance of vertical mixing as a control on rates of DOC photochemical conversion to CO_2 when there are many sunlight-absorbing suspended sediment in the water column. Our study validates well-mixed assumptions used in prior work for most but not all arctic streams and rivers. We assess the features of arctic waters where mixing should be considered (*e.g.*, glacial-fed rivers or thermokarst lakes containing high loads of suspended sediment). These results improve our understanding and estimation of sunlight-driven CO_2 emissions from freshwaters, which is needed to predict how the arctic carbon cycle will respond to climate change.

1. Introduction

Inland waters process substantial amounts of dissolved organic carbon (DOC),[1] such that CO_2 is supersaturated in inland waters with respect to the atmosphere.[2,3] From arctic inland waters, 32–40 Tg per year of DOC is exported to the oceans while 40–84 Tg per year of C is released as CO_2 to the atmosphere.[4–7] CO_2 evasion from inland waters of the Arctic account for up to 40% of net CO_2 exchange between land and air.[1,5] CO_2 production in inland waters is typically attributed to biological respiration of

[a]*Civil and Environmental Engineering, Northwestern University, Evanston, IL, USA*
[b]*Lyles School of Civil Engineering, Purdue University, West Lafayette, IN, USA. E-mail: aubeneau@purdue.edu*
[c]*Civil and Environmental Engineering, Utah State University, Logan, UT, USA*
[d]*Earth and Environmental Sciences, University of Michigan Ann Arbor, Ann Arbor, MI, USA*
[e]*Civil & Environmental Engineering and Earth Sciences, University of Notre Dame, Notre Dame, IN, USA*

† Electronic supplementary information (ESI) available: Additional details on methods and results. 20 pages; 4 tables; 5 figures. See DOI: 10.1039/c8em00455b

DOC,[8] but in inland waters of the Arctic, permafrost DOC is very photoreactive[9–12] such that photochemical processing of DOC is substantial.[9,13–16] Photomineralization, the complete oxidation of DOC to CO_2 by sunlight, currently contributes one third of the CO_2 emitted from arctic inland waters.[13]

Photomineralization is one of several photochemical reactions initiated by the absorption of ultraviolet (UV) light by chromophoric dissolved organic matter (CDOM). As CDOM absorbs UV light, it is broken down (*i.e.*, photobleaching) and some CDOM is completely oxidized to CO_2 (photomineralization). Photomineralization rates are controlled by the photon flux from sunlight, the absorption of photons by CDOM, and the photo-lability (also known as apparent quantum yield) of CDOM to photomineralization.[13] Within a waterbody, the amount of CO_2 produced by photomineralization is also controlled by CDOM residence time, which defines total light exposure of CDOM in the waterbody.[14] Photomineralization rates will be light-limited when sunlight is insufficient under high CDOM amounts and short residence times, and substrate (CDOM) limited when sunlight is in excess under low CDOM amounts and long residence times.[14] The rate-limiting process can shift over time.

Light-attenuating constituents control how photon flux changes with depth in the water column, thereby controlling the integrated rate of photomineralization over the water column, which we refer to here as the depth-integrated photomineralization rate. CDOM is the dominant constituent that attenuates UV and visible light in most arctic waters,[9,13,17] but suspended sediment (SS) also contributes considerably to light attenuation in some arctic and temperate waters, depending on the properties of the watershed over the ice-free summer season.[13,18,19] Attenuation of UV light by water is often negligible due to the high UV attenuation by CDOM in arctic waters.[20,21] In general, light attenuating SS consists of phytoplankton and non-algal SS.[21] Due to the nutrient-poor environment, phytoplankton in arctic lakes generally has a negligible impact on light attenuation.[22,23] Non-algal SS in arctic waters are primarily organic particles from permafrost erosion and inorganic glacial flour, and can strongly influence light attenuation, especially photosynthetically available radiation (PAR) in some arctic waters (*e.g.*, the Mackenzie River and many lakes in the Mackenzie Delta[20,24]). During spring thaw, glacial flour can cause substantial light attenuation in some rivers and lakes that receive high loads from glacial meltwater.[25,26]

Photomineralization is also controlled by hydrologic processes that redistribute CDOM within the water column. Hydrologic controls on the depth-integrated photomineralization rate have received little conceptual and experimental characterization.[27,28] The depth-integrated photomineralization rate depends on the vertical distribution of light and CDOM. Because light intensity decreases through the water column, photomineralization will deplete CDOM in the upper part of the water column when there is no resupply of CDOM to this region.[27,29,30] Therefore, resupply of CDOM from the lower part of the water column to the sunlit surface water by vertical hydrodynamic mixing should increase CDOM loss. Vertical mixing has been found to increase the rate of CDOM photomineralization in mesocosms.[28] Vertical hydrodynamic mixing in inland waters generally ranges over several orders of magnitude.[31–33] Current estimates of photomineralization rates have assumed that CDOM is well-mixed throughout the water column[9,14,34,35] or that photomineralization only occurs in specific layers within the water column.[36] Given that the effect of vertical mixing has been shown to influence other light-dependent surface processes (*e.g.*, primary production in the ocean[27,37]), there is a clear need to evaluate the effect of vertical mixing on depth-integrated photomineralization in freshwaters.

The objective of this study is to model mixing limitations on photomineralization in freshwater systems, *i.e.*, whether and by how much vertical mixing limits the depth-integrated photomineralization rate. This work includes both conceptual and quantitative models. The conceptual model considers the factors that control mixing limitations on photomineralization. We also quantify the extent to which vertical mixing limits photomineralization for cases where the light profile can be approximated as exponential. For this case, we present a reactive-transport model that integrates vertical hydrodynamic mixing with an existing photomineralization model. This quantitative model provides a rigorous and consistent way to delineate factors that control the extent of mixing limitation on photomineralization for a range of waterbodies, and to identify system conditions under which the well-mixed assumption is not appropriate for estimation of photomineralization rates. Finally, we use this model to assess mixing limitations in arctic rivers, streams, and lakes.

2. Methods

2.1 Conceptual model

To answer the question whether and by how much vertical mixing affects photomineralization throughout the water column, we categorize waterbodies based on composition and the overall structure of light attenuating constituents, *i.e.*, whether CDOM is the only light attenuating constituent, and whether the light attenuating constituents are generally homogeneous in the water column. Based on understanding of the effects of each factor on the depth-integrated photomineralization rate, we infer the potential for mixing-induced limitation on photomineralization for each of the four categories (Fig. 1A). This model provides a conceptual framework to cover the conditions needed to evaluate mixing limitations.

When CDOM is the only light-attenuating constituent, CDOM can be either homogeneously distributed or nonuniformly distributed in the water column. In the former case (upper left quadrant in Fig. 1A), light decays exponentially with depth.[38] Homogeneous CDOM structure implies that CDOM is well-mixed in the water column, hence yielding no mixing limitation. When CDOM is nonuniformly distributed in the water column (upper right quadrant in Fig. 1A), light attenuation varies with depth following the distribution of CDOM, and hence cannot be generalized as exponential.[38] Because no other constituent attenuates light in these cases, the total photomineralization rate over the water column depends on the total amount of light attenuated over the water column, which

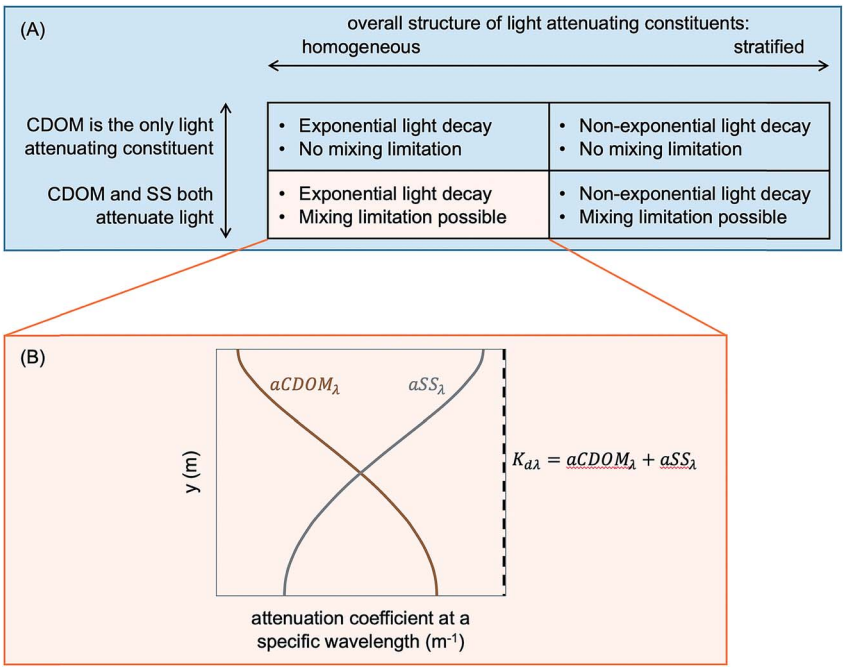

Fig. 1 (A) Conceptual diagram of the four quadrants determining mixing limitations. The four quadrants are defined by composition (whether CDOM is the only light attenuating constituent) and overall structure of light attenuating constituents (whether the total light attenuation coefficient is homogeneous with depth). (B) Example distributions of light attenuation coefficient of CDOM ($aCDOM_\lambda$), light attenuation coefficient of suspended sediment (SS) (aSS_λ), and total light attenuation coefficient ($K_{d\lambda}$) as a function of the vertical position in the water column (y). This example corresponds to the lower left quadrant of (A), with homogeneous light attenuation when CDOM and SS both attenuate light. This example shows that light attenuation can be homogeneous over depth even when CDOM is not homogeneously distributed.

depends on the total amount of CDOM present in the water column. In this case, the concentration distribution of CDOM only affects where the light is absorbed, not the total amount of light absorbed throughout the water column. Therefore, vertical mixing does not affect photomineralization in these systems. Photomineralization behavior for this case is described in more details in the ESI (Section SI-1).† Because CDOM is the dominant light-attenuating constituent in most arctic waters,[9,13] the well-mixed assumption is valid for most arctic systems.

When CDOM and SS both attenuate light, their vertical distribution controls the decay of light over depth. SS in the well-lit surface of the water column can attenuate light independently of CDOM, such that light attenuation over depth does not necessarily follow the distribution of CDOM. In this case, SS influences the amount and spectrum of sunlight available to photomineralize CDOM. Therefore, in poorly-mixed systems with significant SS, attenuation of light by SS shelters CDOM from photomineralization. The sheltered CDOM not only receives less light, but may also receive lower-energy photons (longer wavelengths), which are less photo-reactive. This sheltering of CDOM results in less photomineralization over the water column compared to the well-mixed scenario.

When the vertical distribution of light-attenuating constituents (SS and CDOM) is relatively homogeneous in the water column, the light profile can be approximated as an exponential decrease with depth[38] (lower left quadrant in Fig. 1A). This case is quantitatively analyzed here (in Section 2.3). Because both CDOM and SS attenuate light, light attenuation constituents can be homogeneous with depth even when the CDOM and SS concentration distributions are not. For example, a water column with less CDOM near the surface can still have uniform light attenuation and therefore an exponential vertical profile of light, as long as SS is higher in the surface water (Fig. 1B). The scenario where CDOM is poorly mixed and shaded by SS, yet the light profile is still approximately exponential, can be found in some arctic streams and ponds where fine SS is introduced into the waters by glacier meltwater and permafrost erosion.[9,21,25,39,40]

When SS and CDOM are stratified in the water column (lower right quadrant in Fig. 1A), the light profile will not be exponential.[38] In this case, CDOM can be sheltered from light in a way similar to the lower-left quadrant, although this scenario is much more complex due to the highly non-uniform distributions of CDOM and SS in the water column, and correspondingly complex light profile. Mixing limitation is thus also possible in this quadrant, but quantitative analysis of this case is beyond the scope of the current study.

2.2 Field data

We use field data in combination with a reactive-transport model to quantify mixing limitations in waterbodies that exhibit exponential light attenuation over depth, corresponding to the lower-left quadrant of Fig. 1A. The model is first applied to the Kuparuk River, Alaska, as a proof-of-concept because of the extensive data available in this system (Table S1†). The model is then generalized to assess mixing limitations in other

arctic waters using photochemical and hydrological parameters from prior studies (Table S1†). Parameters needed for the photochemical modeling, such as CDOM concentrations, were compiled from 20 studies, of which the largest dataset includes measurements from 70 lakes and 73 rivers in the North Slope of Alaska.[13]

The Kuparuk River has been the focus of research on aquatic carbon cycling and river hydrology for the past ~30 years as part of the NSF Arctic Long Term Ecological Research (LTER) program. The Kuparuk River originates in the northern hills of the Brooks Range and flows about 320 km northward to the Arctic Ocean (Fig. S1†). The river flows from mid-May to October.[41] Up to 80% of the annual discharge is spring snowmelt, and peak discharge can occur during large storm events in the summer.[42] The rivers in this and other watersheds on the North Slope of Alaska are open-canopy with 24 hour sunlight in summer, and typically have shallow flows and the larger rivers have gravel-to-boulder beds.[43,44] The Kuparuk watershed is underlain by continuous permafrost 250 to 600 m in depth.[45,46] Light attenuation in the Kuparuk River results primarily from absorption by CDOM,[13] and UV light has been previously shown to decay exponentially with depth in the water column.[13] This corresponds to the upper left quadrant in Fig. 1A, where no mixing limitation is expected.

Photochemistry data were collected from the Kuparuk River basin over the summers of 2011–2013.[13] This dataset includes wavelength (λ) specific spectra of hourly photon flux at the water surface ($Q_{\mathrm{dso}\text{-}\lambda}$), the apparent quantum yield describing the photo-lability of CDOM to photomineralization (ϕ_λ) with ±95% confidence intervals, the light attenuation coefficient of CDOM (aCDOM_λ) with ±95% confidence intervals, and empirical parameters α_λ and ε_λ that relate DOC concentration to the light attenuation coefficient of CDOM. The light attenuation coefficient describes the amount of CDOM, which is strongly, positively correlated to DOC concentration but cannot be quantified on a per C basis. DOC concentrations ranged from 0.39–0.57 mol C m^{-3} (Cory *et al.* 2014, Table S1†). River discharge and river channel geometry were measured during flow seasons in 2013–2015 at 8 gauging stations along the main-stem Kuparuk[47] (Fig. S1†). In the three-year record, river discharge (Q) ranged between 0.08 $\mathrm{m}^3\ \mathrm{s}^{-1}$ at baseflow in the upper Kuparuk to 126.4 $\mathrm{m}^3\ \mathrm{s}^{-1}$ during peak flow in the lower Kuparuk. Water column depth (H) ranged from ~0.1 to 3 m, at least 10 times smaller than river widths (W) (Fig. S2†). Water surface slope (S) was estimated using a 5 m DEM.[48] The broad ranges of photochemistry and hydrology conditions in the Kuparuk River basin are summarized in Fig. S2.† Notation used in this study is summarized in Table S3.†

Because there is less data from other arctic waters compared to the Kuparuk River, we grouped arctic waters into rivers (stream order > 3), streams (stream order ≤ 3, including chutes of beaded streams), beaded streams (pools, excluding chutes), and lakes. For these groups we compiled ranges of DOC concentration (C = 0.028–18 mol m^{-3} in streams and rivers, 0.12–3.1 mol m^{-3} in beaded streams, and 0.008–2.7 mol m^{-3} in lakes), photo-lability of CDOM ($\phi_{300} = 4 \times 10^{-4}$ to 0.08 in rivers, 5×10^{-4} to 0.04 in streams, 0.003–0.04 m^{-1} in beaded streams, and 4×10^{-4} to 0.08 in lakes), the light attenuation coefficient of CDOM (aCDOM_{300} = 3.6–103 m^{-1} in rivers, 4.6–334 m^{-1} in streams, 33–359 m^{-1} in beaded streams, and 4.3–79 m^{-1} in lakes), and water column depth (H = 0.14–15.5 m in rivers, 0.015–2.1 m in streams, 0.12–3 m in beaded streams, and 0.08–43 m in lakes) from 40 studies and datasets (Table S1†). We used the same photon flux spectra reaching the water surface for all arctic waters in this study given that all waters were in the same region of the Alaskan Arctic near the Kuparuk River. Of the arctic streams, rivers, and lakes where spectra of photochemical parameters were available from a dataset of 70 lakes and 73 streams and rivers,[13] the average depth at which 99% of the UV light is attenuated (known as the $Z_{1\%}$) was 0.1 m in stream and rivers and 0.2 m in lakes at 300 nm, or 0.4 m in streams and rivers and 1.4 m in lakes at 412 nm. Compared to the relatively shallow water column of these systems (mean depths < 1 m for stream and rivers, ~2 m for lakes),[13] on average UV light at 300 nm penetrates about 20% of the water column, while longer wavelength UV light at 412 nm can reach the bottom of the water column. In addition, for arctic streams, rivers, and beaded streams, we compiled ranges of water surface slope ($S = 5 \times 10^{-5}$ to 0.03 in rivers, 1.7×10^{-4} to 0.1 in streams, and 3×10^{-4} to 0.009 in beaded streams) and flow discharge (Q = 0.7–128 769 $\mathrm{m}^3\ \mathrm{s}^{-1}$ in rivers, 0.005–52 $\mathrm{m}^3\ \mathrm{s}^{-1}$ in streams, and 0.000024–1.73 $\mathrm{m}^3\ \mathrm{s}^{-1}$ in beaded streams); for arctic lakes, we compiled ranges of Secchi depth (S_d = 0.3–11.2 m), based on which the average epilimnion depth of arctic lakes was estimated (4.3 m). Data compilation are detailed in the ESI (Section SI-2).† Sources and ranges of these compiled data are summarized in Tables S1 and S2,† respectively. Arctic waters have low electrical conductivity, are weakly buffered (low carbonate alkalinity), and are supersaturated with CO_2 with respect to atmospheric pressures.[7] As a result, we assume that CO_2 produced by photomineralization exchanges readily with the atmosphere.

SS can account for up to 50% of light attenuation in glacial-fed rivers, thermokarst, or other SS-rich lakes.[9,13,24,49] Thus we assumed that the total light attenuation coefficient ranges between 1–2 times the measured aCDOM_λ for each type of arctic systems (Table S2†). However, this assumption does not consider the different attenuation spectra of SS compared to CDOM. SS attenuates more light in the visible (PAR) region than in the UV, in contrast to CDOM, which attenuates more UV than visible light.[50] We also did not consider light scattering by SS, which increases the effective pathlength for photons during downward propagation.[51,52] Our characterization of SS attenuation thus overestimates the sheltering effect of SS, so that the mixing limitations predicted by our model represent maximum estimates.

2.3 Quantitative model

To assess the effect of vertical hydrodynamic mixing on depth-integrated photomineralization rate, we use a dispersion-reaction model that extends the existing photomineralization model with vertical dispersion. Field observations indicated that lateral (bank to bank) gradients of DOC concentration were

small, so we assume no lateral transport of DOC in this model. We assume steady, uniform flow, and therefore solve for the vertical distribution of DOC concentration in the water column (with change in DOC concentration based on its relationship to CDOM as described below):

$$\frac{\partial C(y,t)}{\partial t} = \frac{\partial}{\partial y}\left(D(y)\frac{\partial C(y,t)}{\partial y}\right) - \sum_{\lambda}\phi_{\lambda}\mathrm{aCDOM}_{\lambda}(y,t)Q_{\mathrm{dso}\text{-}\lambda}\mathrm{e}^{-K_{\mathrm{d}\lambda}(y)y} \quad (1)$$

with no-flux boundary conditions

$$\left.\frac{\partial C(y,t)}{\partial y}\right|_{y=0} = 0 \quad (2a)$$

$$\left.\frac{\partial C(y,t)}{\partial y}\right|_{y=H} = 0 \quad (2b)$$

where $C(y,t)$ is DOC concentration, t is time, y is the vertical position that is 0 at water surface and positive in the downward direction, and $D(y)$ is the vertical dispersion coefficient that dictates vertical mixing and sets the rate of resupply of CDOM from bottom waters to the surface. Additional factors that influence the distribution of CDOM over depth, such as thermal stratification in arctic beaded streams and lakes,[53–55] are not considered here. The photomineralization rate is the product of ϕ_{λ}, $\mathrm{aCDOM}_{\lambda}(y,t)$, $Q_{\mathrm{dso}\text{-}\lambda}$, and the attenuation of photon flux governed by the total light attenuation coefficient $K_{\mathrm{d}\lambda}(y)$ over depth.[13] Photo-lability of CDOM (ϕ_{λ}) may decrease over time due to depletion of reactive moieties, but how photo-lability changes over time and downstream distance is unknown,[13] so we assume that photo-lability stays constant over depth and over time. Other factors such as temperature, pH, iron, and nitrate may also influence photo-lability of CDOM and thus photomineralization rates,[14,56–58] but these factors are not considered in this study. We track changes of DOC concentration in this model following the empirical relationship $\mathrm{aCDOM}_{\lambda} = \begin{cases} \alpha_{\lambda} + \varepsilon_{\lambda}C & \text{if } \alpha_{\lambda} + \varepsilon_{\lambda}C > 0 \\ 0 & \text{if } \alpha_{\lambda} + \varepsilon_{\lambda}C \le 0 \end{cases}$ derived from measurements of aCDOM_{λ} and C from 70 arctic lakes and 73 arctic streams and rivers.[13] It should be noted that this relationship may change over time due to the fact that high solar exposure causes loss of CDOM absorbance without a decrease in DOC (photobleaching).[16,59] As CDOM is photobleached, rates of UV light attenuation by CDOM and thus rates of DOC photomineralization will decrease over time. However, the effect of faster loss of CDOM than DOC is expected to have a relatively small effect on quantification of DOC photomineralization in arctic freshwaters where DOC photomineralization is often light-limited[14] and where the majority of DOC (>50%) is chromophoric.[13] Thus, over the relatively short time scales (*i.e.*, daily rates) of DOC photomineralization considered in the present study, there is not enough UV exposure to bleach away enough CDOM to substantially slow rates of photomineralization. For the scope of this study, we assume that the relationship between aCDOM_{λ} and C stays constant over time. Note that α_{λ} is negative, so positive attenuation at zero C would never occur. The goal is to solve for the depth-integrated photomineralization rate (r), defined as the first order reaction rate of the depth-averaged DOC concentration ($\langle C(y,t)\rangle$)

$$\frac{\mathrm{d}\langle C(y,t)\rangle}{\mathrm{d}t} \equiv r\langle C(y,t)\rangle \quad (3)$$

In order to compare the effect of mixing on photomineralization in freshwaters that exhibit exponential light attenuation over depth, we group the dimensional parameters in (1) using non-dimensionalization, a theoretical tool commonly used to reduce the number of dimensional parameters in a model into a smaller and more manageable set of dimensionless parameters.[60] (1) becomes

$$\frac{\partial C^*(y^*,t^*)}{\partial t^*} = \frac{\partial}{\partial y^*}\left(\frac{D(y^*)}{\langle D\rangle}\frac{\partial C^*(y^*,t^*)}{\partial y^*}\right) - \sum_{\lambda} d_{\lambda}^* \mathrm{e}^{-p_{\lambda}^* y^*} C^*(y^*,t^*) \quad (4)$$

with no-flux boundary conditions

$$\left.\frac{\partial C^*(y^*,t^*)}{\partial y^*}\right|_{y^*=0} = 0 \quad (5a)$$

$$\left.\frac{\partial C^*(y^*,t^*)}{\partial y^*}\right|_{y^*=1} = 0 \quad (5b)$$

where superscript * indicates dimensionless variables, $\langle D\rangle$ is the depth-averaged vertical dispersion coefficient, and d_{λ}^* and p_{λ}^* are wavelength-specific dimensionless parameters defined by $d_{\lambda}^* = \frac{H^2}{\langle D\rangle}\phi_{\lambda}\frac{\mathrm{aCDOM}_{\lambda}(y^*,t^*)}{C(y^*,t^*)}Q_{\mathrm{dso}\text{-}\lambda}$ and $p_{\lambda}^* = K_{\mathrm{d}\lambda}(y^*)H$. Each dimensionless parameter represents the relative strength of competing processes. For example, a higher dimensionless dispersion coefficient d_{λ}^* indicates greater loss rate of CDOM by photomineralization at the water surface relative to the resupply rate of CDOM by vertical dispersion to the water surface. A greater dimensionless light decay coefficient, p_{λ}^*, indicates greater attenuation of light with depth in the water column. Non-dimensionalization of these different processes and systems can be compared in a self-consistent framework.[61] The steps of non-dimensionalization are detailed in the ESI (Section SI-3).†

We further assume that light profile over depth can be generalized as exponential, which corresponds to the left quadrants of Fig. 1A. Exponential light profile means that total light attenuation coefficient is constant over depth at each wavelength: $K_{\mathrm{d}\lambda}(y^*) = K_{\mathrm{d}\lambda}$, so that p_{λ}^* is constant over depth at each wavelength. Given that $\frac{\mathrm{aCDOM}_{\lambda}(y^*,t^*)}{C(y^*,t^*)}$ is approximately constant, d_{λ}^* is also constant at each wavelength. We then eliminate the wavelength dependency of d_{λ}^* and p_{λ}^* by fitting the reaction term exponentially with dimensionless vertical position (y^*). (4) becomes

$$\frac{\partial C^*(y^*,t^*)}{\partial t^*} = \frac{\partial}{\partial y^*}\left(\frac{D(y^*)}{\langle D\rangle}\frac{\partial C^*(y^*,t^*)}{\partial y^*}\right) - d^*\mathrm{e}^{-p^* y^*} C^*(y^*,t^*) \quad (6)$$

where d^* represents a dimensionless first-order reaction rate coefficient at the water surface, and p^* represents a dimensionless decay coefficient of reaction with depth. Specifically, d^* is the ratio of the photomineralization rate at the water surface to the vertical mixing rate, which is a form of dimensionless Damkohler number.[62,63] Because this Damkohler number is evaluated at the water surface ($y^* = 0$), we refer to d^* as the surface Damkohler number. The magnitude of d^* reflects the surface loss of CDOM by photomineralization relative to resupply of CDOM by vertical mixing to the water surface, and thus provides information about how CDOM resupply limits the depth-integrated photomineralization rate when SS is present to shelter CDOM from light (lower left quadrant). Dimensionless coefficient p^* depends on the ratio of the actual water column depth to a characteristic attenuation depth, which represents the ensemble photon attenuation over all wavelengths from the water surface to bed sediments. We therefore refer to p^* as the dimensionless light attenuation. The magnitude of p^* indicates the extent of UV attenuation through the water column by SS and CDOM, and thus provides information on how light penetration limits the depth-integrated photomineralization rate when SS is present to shelter CDOM from light (lower left quadrant).

Eqn (5)–(6) do not have a steady-state solution, due to the ongoing disappearance of DOC mass by photomineralization. However, after sufficiently long time (or equivalently, sufficiently long downstream distance), the depth-integrated photomineralization rate is relaxed from the initial distribution of DOC, such that depth-integrated photomineralization rate can be well-approximated by a first-order rate constant.[64] This is known as the asymptotic behavior. At the asymptotic regime, the dimensionless depth-averaged DOC concentration decays at a first-order rate constant over time[64]

$$\frac{\mathrm{d}\langle C^*(y^*,t^*)\rangle}{\mathrm{d}t^*} = r^*\langle C^*(y^*,t^*)\rangle \tag{7}$$

Eqn (7) is the dimensionless equivalent of (3), where r^* is the dimensionless depth-integrated photomineralization rate. The depth-integrated photomineralization rate under asymptotic regime represents the depth-integrated loss rate of DOC under the vertical distribution of DOC that is established over time. We employ the moment method,[64,65] detailed in the ESI (Section SI-4),† that solves for r^* and vertical distribution of DOC from (5)–(6) defined by d^* and p^*.

Note that r^* and the depth average of the first-order reaction term $d^*\mathrm{e}^{-p^*y^*}$ in (6) are only the same under well-mixed conditions, because dimensionless DOC concentration is dependent on the dimensionless vertical position. In contrast, assuming *a priori* that the water column is well mixed, *i.e.*, $C^*(y^*,t^*) = \langle C^*(y^*,t^*)\rangle$, yields

$$r^*_{\mathrm{wm}} = \frac{d^*}{p^*}\left(1-\mathrm{e}^{-p^*}\right) \tag{8}$$

r^*_{wm} is the maximum possible rate for r^*, because there is no sheltering of CDOM from light in this case. To quantify the extent by which vertical mixing limits the depth-integrated photomineralization rate, we define reaction efficiency (η_{react}) as the ratio of the depth-integrated photomineralization rate without and with the well-mixed assumption:[66,67]

$$\eta_{\mathrm{react}} = \frac{r^*}{r^*_{\mathrm{wm}}} \tag{9}$$

The reaction efficiency ranges from 0 to 1. We categorize $\eta_{\mathrm{react}} > 0.9$ to indicate no substantial limitation, $\eta_{\mathrm{react}} < 0.5$ to indicate substantial limitation, and $0.5 < \eta_{\mathrm{react}} < 0.9$ to indicate partial limitation on the depth-integrated photomineralization rate. Each combination of d^* and p^* defines a r^* and r^*_{wm}, and hence defines a η_{react}. Note that results of $\eta_{\mathrm{react}} < 1$ apply only for the lower left quadrant when SS is present to shelter CDOM from light and thus influence loss of CDOM from photomineralization.

2.4 Evaluating the well-mixed assumption in arctic waters

First, we plot the reaction efficiency as a function of all possible combinations of surface Damkohler number (d^*) and dimensionless light attenuation (p^*). Each possible combination of d^* and p^* corresponds to a unique point in the plot. We call the 2-dimensional space defined by d^* and p^* coordinates as the phase space of η_{react}. The phase space of η_{react} reflects how well the well-mixed assumption estimates the depth-integrated photomineralization rate under different mixing and light attenuation conditions. From (6), $\frac{D(y^*)}{\langle D\rangle}$ defines different scaling of d^* for different types of arctic systems (Fig. S5†). For comparison, we rescale d^* for different types of arctic systems to have the same magnitude of η_{react} at $d^* = 10$ and $p^* = 10$ as the streams and rivers type, so that d^* and p^* pairs from different system types are directly comparable. Vertical dispersion profiles ($D(y^*)$) for different types of arctic systems are detailed in the ESI (Section SI-5).†

Second, we estimate d^* and p^* values for each type of arctic water, and then plot the d^* and p^* combinations onto the phase space. For the Kuparuk River, the measured aCDOM$_\lambda$ approximates the total light attenuation coefficient ($K_{\mathrm{d}\lambda}(y)$) over depth well.[13] To estimate d^* and p^* values for other arctic systems, we estimate d^*_λ and p^*_λ from DOC concentration and aCDOM$_\lambda$ data (Table S1†), approximate the fraction $\frac{\mathrm{aCDOM}_\lambda(y^*,t^*)}{C(y^*,t^*)}$ in d^*_λ as constant over depth, and then fit the reaction term in (4) to the exponential form in (6).

Finally, we estimate the percentage of arctic waters that are partially limited and substantially limited by vertical mixing. We assume that each photochemical and hydrological parameter has log-uniform distribution, which is a commonly used assumption when the underlying distributions of input parameters are unknown and input parameters have wide ranges of values.[68–70] The percentage of mixing-limited waters will serve as a rough estimate, dependent on the log-

uniform assumption. For each water, we calculate the ratio of depth-integrated light attenuation by CDOM and the depth-integrated light attenuation by all constituents, $\frac{\int_{y=0}^{H}\sum_{\lambda}\mathrm{aCDOM}_{\lambda}(y)\mathrm{e}^{-K_{\mathrm{d}\lambda}y}\mathrm{d}y}{\int_{y=0}^{H}\sum_{\lambda}K_{\mathrm{d}\lambda}\mathrm{e}^{-K_{\mathrm{d}\lambda}y}\mathrm{d}y}$, which we call the depth-integrated attenuation ratio. $\mathrm{aCDOM}_{\lambda}(y)$ is estimated from the vertical distribution of DOC concentration at asymptotic regime (Section SI-4†) and the empirical scaling between DOC concentration and aCDOM_{λ},[14] assuming that measured aCDOM_{λ} corresponds to the mean value of aCDOM_{λ} over depth.

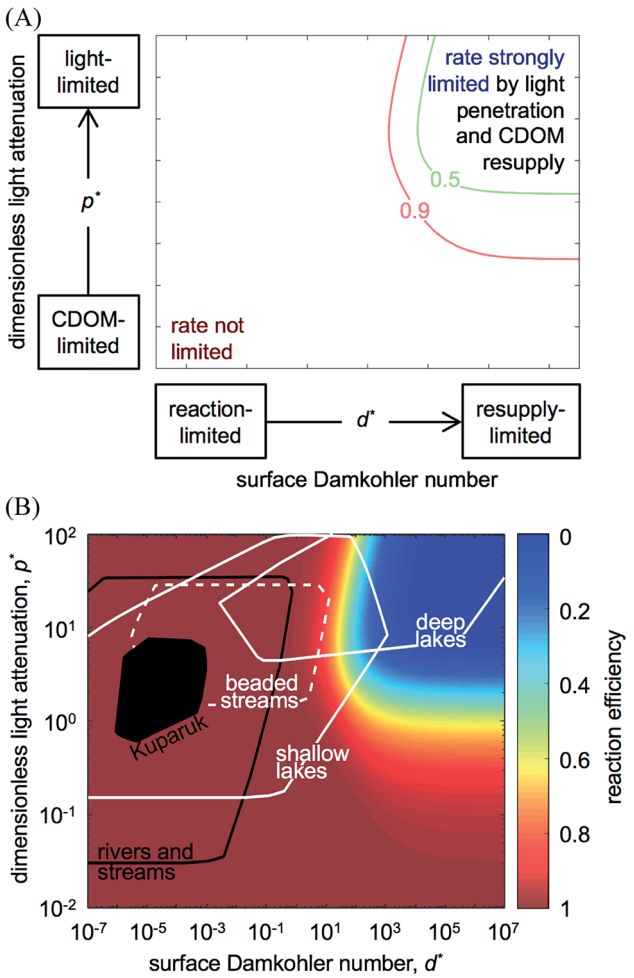

Fig. 2 Mixing and light penetration limitations on CDOM photomineralization in arctic surface waters, presented in the phase space defined by the surface Damkohler number (d^*) and the dimensionless light attenuation (p^*). (A) As d^* increases, photomineralization near the water surface switches from being limited by the CDOM reaction rate to being limited by the CDOM resupply rate. As p^* increases, photomineralization in the water column switches from being limited by CDOM amount to being limited by UV light availability. Isopleths represent reaction efficiency values. (B) Same as (A), but the shading indicates the reaction efficiency (η_{react}). This analysis indicates that the Kuparuk River is well-mixed for photomineralization under the observed conditions. CDOM is generally expected to be well-mixed in arctic streams, rivers, and fast-flowing beaded streams. However, the well-mixed assumption is expected to fail in deeper arctic lakes and slow-flowing beaded streams that exhibit strong light attenuation and weak vertical mixing.

3. Results

3.1 Factors controlling the extent of mixing limitation

Fig. 2 shows the reaction efficiency (η_{react}) as a function of surface Damkohler number (d^*) and dimensionless light attenuation (p^*) when light decays exponentially with depth. We verified the theoretical expectation of no mixing limitation when CDOM is the only light-attenuating constituent (ESI Section SI-1†), so the following results focus on two cases (1) when both CDOM and SS attenuate light, *i.e.*, attenuation ratio < 1 and (2) a proof of concept result for Kuparuk River where the model results should confirm no mixing limitation due to lack of SS and rapid mixing in the river.

For the first case, when the surface Damkohler number d^* is smaller than 1, the resupply rate of CDOM is greater than the photomineralization rate of CDOM at the water surface, so the depth-integrated photomineralization rate is not limited by mixing (Fig. 2). When the surface Damkohler number is higher than 1, slower resupply of CDOM results in steeper gradients of CDOM with depth, which enhances the sheltering of CDOM from light at depth by SS in the surface. As the surface Damkohler number increases, the depth-integrated photomineralization rate is increasingly limited by the slow resupply of CDOM (Fig. 2A). The reaction efficiency decreases monotonically with surface Damkohler number at any level of dimensionless light attenuation (Fig. 2B and 3A), suggesting that larger surface Damkohler number reflects higher mixing limitation.

Low values of dimensionless light attenuation ($p^* \ll 10^{-1}$) reflect low attenuation of UV light by CDOM and SS over depth. Abundant light reaching deeper water indicates that the depth-integrated photomineralization rate is not limited by UV light at depth, but is limited by the amount and photo-lability of CDOM[14] (Fig. 2A). Low light attenuation means little sheltering of CDOM from light, such that reaction efficiency is close to 100% (Fig. 2B and 3B). Mixing limitation is therefore minimal when dimensionless light attenuation is very low. As dimensionless light attenuation increases, stronger sheltering of CDOM from light by SS indicates that the depth-integrated photomineralization rate is increasingly limited by UV light availability at depth (Fig. 2A). The reaction efficiency decreases substantially with dimensionless light attenuation (Fig. 2B and 3B), indicating higher mixing limitation. As dimensionless light attenuation continues to increase ($p^* > \sim 10^1$), strong light attenuation starts to diminish UV light immediately below the water surface, leaving almost the entire water column dark. This leads to little photomineralization in almost the entire water column, which means that CDOM distribution becomes more uniform as dimensionless light attenuation continues to increase ($p^* > \sim 10^1$). Reaction efficiency, after decreasing with dimensionless light attenuation, increases again (Fig. 2B and 3B), suggesting less mixing limitation once dimensionless light attenuation is very large.

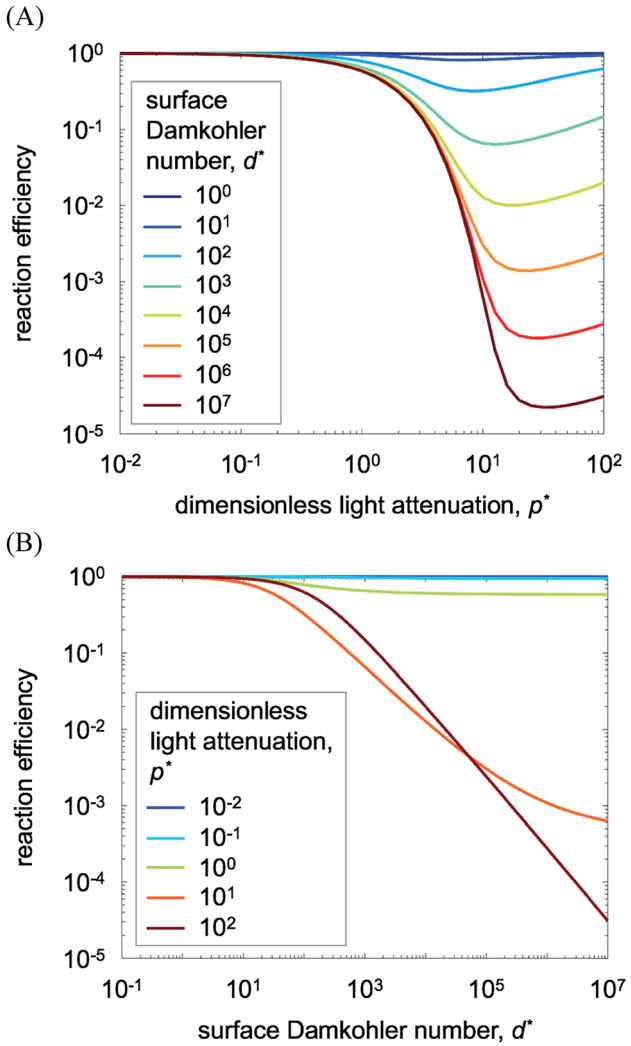

Fig. 3 Effects of surface Damkohler number (d^*) and dimensionless light attenuation (p^*) on photomineralization reaction efficiency. (A) Reaction efficiency as a function of p^*. Colored lines indicate different d^* values. For any value of d^*, reaction efficiency decreases with increasing p^*, reaches a trough, and slightly returns back. (B) Reaction efficiency as a function of d^*. Colored lines indicate different p^* values. For any value of p^*, reaction efficiency decreases with increasing d^* monotonically. The well-mixed assumption (low reaction efficiency) is generally invalid when dimensionless light attenuation (p^*) and surface Damkohler number (d^*) are both high.

When the surface Damkohler number (d^*) or dimensionless light attenuation (p^*) is small ($d^* < 5$ or $p^* < 0.2$), mixing limitation is not substantial ($\eta_{react} > 90\%$) (Fig. 2). Rapid resupply of CDOM or abundant penetration of UV light ensures that the well-mixed assumption approximates the depth-integrated photomineralization rate moderately well. When the surface Damkohler number and dimensionless light attenuation are larger ($5 < d^* < 40$ and $0.2 < p^* < 1.3$), the depth-integrated photomineralization rate is partially limited by vertical mixing ($50\% < \eta_{react} < 90\%$) (Fig. 2). Both the resupply rate of CDOM and the penetration of UV light start to invalidate the well-mixed assumption. When the surface Damkohler number and dimensionless light attenuation are both large ($d^* > 40$ and $p^* > 1.3$), mixing limitation is substantial ($\eta_{react} < 50\%$) (Fig. 2), such that CDOM is poorly mixed in the water column. The well-mixed assumption is expected to fail when light attenuation over depth is strong (high p^*) and when water surface photomineralization rate exceeds the resupply rate of CDOM (high d^*).

3.2 Mixing limitation in different arctic surface waters

Under the observed natural variations in the main stem of the Kuparuk River (Fig. S2†), the estimated surface Damkohler number (d^*) ranges from 8.5×10^{-7} to 9.1×10^{-4}, at least 3 orders of magnitude lower than the threshold of $d^* = 1$ where mixing limitation may be possible (Fig. 2B). This result is expected from the conceptual model showing that photomineralization over the main-stem Kuparuk River is not limited by mixing due to the fact that CDOM is the main UV-attenuation constituent (Fig. 1A). Under these conditions, photomineralization is constrained by insolation, CDOM amount, and CDOM photo-lability.[14]

Other arctic streams and rivers (including chutes of beaded streams) are expected to have well-mixed CDOM under reported natural variations in hydrology and photochemistry ($\eta_{react} = 100\%$) (Fig. 2B). The surface Damkohler number of arctic streams and rivers ($3.3 \times 10^{-9} < d^* < 0.7$) is always below the threshold of 1, indicating that vertical mixing is always strong enough to resupply CDOM to the surface. None of the arctic streams and rivers modeled in this study are partially or strongly limited by mixing. Because CDOM is always well-mixed, the depth-integrated attenuation ratio is the same as the assumed proportion between $aCDOM_\lambda$ and total light attenuation $K_{d\lambda}$, which ranges from 0.5 to 1. Compared to arctic streams and rivers, arctic beaded streams (pools, excluding chutes) generally have higher values of surface Damkohler number and dimensionless light attenuation, indicating that there may be more mixing limitation than arctic streams and rivers due to the limited resupply of CDOM and attenuation of UV light by SS. However, beaded streams show only minimal to partial mixing limitation ($80\% < \eta_{react} \leq 100\%$) (Fig. 2B). Of the simulated beaded streams, less than 1% are partially limited by mixing and none exhibited substantial mixing limitation. Of the beaded streams partially limited by mixing, the depth-integrated attenuation ratio is 0.92 ± 0.001 on average, meaning that CDOM is the dominant UV-light attenuating constituent, implying a small role of SS in the UV light attenuation, consistent with the model results showing little possibility of mixing limitation in these waters.

Lakes have the largest projected ranges of surface Damkohler number and dimensionless light attenuation. The reaction efficiency ranges from ~10% to 100% in shallow lakes (water column depth < 4.3 m), and from 0.02% to 100% in deep lakes (water column depth ≥ 4.3 m), indicating minimal to substantial mixing limitations (Fig. 2B). Deeper lakes are generally less well-mixed on a whole lake basis than shallow lakes due to greater depth and lower vertical mixing in the deep layer. Overall, 12% of the simulated arctic lake systems are partially limited by mixing and 30% are substantially limited by mixing. These results are due to greater UV-light attenuation by

SS as indicated by an average depth-integrated attenuation ratio of 0.95 ± 0.001 in arctic lakes partially limited by mixing, and 0.58 ± 0.002 in arctic lakes substantially limited by mixing. The percentage of mixing-limited systems and the depth-integrated attenuation ratio for each type of arctic systems are summarized in ESI Table S3.†

When comparing mixing limitation across different systems, the nature of dimensionless coefficients (d^* and p^*) allows us to compare controlling factors on photomineralization among systems with quite different characteristics. For example, waters that have different photo-lability of CDOM, water column depth, and vertical dispersion can have the same mixing limitations (same d^* and p^*). Arctic beaded streams that receive high loads of photo-labile CDOM from land[14,71] and have low vertical dispersion in pools[54,71] may exhibit a small extent of mixing limitation on photomineralization rates. The same mixing limitation can also be representative of arctic lakes that have less labile CDOM[13] but a deeper water column and lower vertical dispersion coefficients.

4. Discussion

The study provides both conceptual and quantitative models to assess the importance of vertical hydrodynamic mixing on the depth-integrated rate of CDOM photomineralization in freshwater systems. When CDOM is the only light-attenuating constituent, which is the case in most arctic freshwater systems,[9,13] vertical mixing does not affect the depth-integrated photomineralization rate. In the presence of light-attenuating SS, vertical mixing should be considered when estimating depth-integrated photomineralization. For SS-influenced waterbodies that exhibit exponential light attenuation over depth, mixing limitation is pronounced when light attenuation over depth is strong and when the rate of CDOM photomineralization is greater than the rate of CDOM replenishment by vertical mixing. While the present study is primarily focused on arctic waters, both the conceptual model and numerical model are directly applicable to temperate waters. CDOM in temperate waters is typically less labile than CDOM in arctic waters,[13,72] and suspended phytoplankton and sediments in temperate waters can play a much more important role in attenuating UV light.[49] Therefore, we expect that mixing limitation will have an important effect on photomineralization rates in temperate waters.

While the present study focuses on vertical hydrodynamic mixing, other factors can also strongly influence the distribution of CDOM over depth in the water column, and hence alter the depth-integrated photomineralization rate. Thermal stratification is known to inhibit vertical mixing in arctic lakes and beaded streams[53–55] as well as temperate lakes.[73,74] Thermal stratification decreases replenishment of CDOM from deep regions of the water column even for shallow arctic lakes (water column depth < 4.3 m),[75] and decreases depth-integrated photomineralization rate.[14] Relative to the exponential light attenuation over depth considered here, mixing inhibition by thermal stratification is expected to further decrease photomineralization rates.

Relatively high mixing and low SS attenuation in most arctic waters mean that well-mixed assumptions used in prior work are valid in many, but not all, of these waters. Our results show that arctic streams and rivers with strong vertical mixing relative to the photomineralization rate show no mixing limitation regardless of how much SS is present. Some arctic beaded streams and lakes have weaker mixing, which limits photomineralization when SS is present. Photomineralization reaction efficiency, estimated from surface Damkohler number and dimensionless light attenuation, can be used to quantify the extent of mixing limitation. We found an average reaction efficiency of 99.8% for beaded streams, indicating negligible mixing limitation on photomineralization. With the well-mixed assumption, our analysis of beaded streams yielded an average depth-integrated photomineralization rate of 26 ± 0.5 mmol C m^{-2} d^{-1}, consistent with the previous estimate of 24.7 ± 18.3 mmol C m^{-2} d^{-1} in Imnavait Creek.[13] For arctic lakes, we found an average reaction efficiency of 80% – indicating that mixing limitations decreased the photomineralization rate by 20% – and a depth-integrated photomineralization rate of 36 ± 1 mmol C m^{-2} d^{-1}. The simulated average photomineralization rate is higher than previously reported rates (9.15 ± 0.50 in coastal plain lakes of arctic Alaska)[13] because the simulated average rate is affected by extremely high values (*i.e.*, very deep lakes with very high CDOM and AQY) given the wide range of photochemical and hydrological parameters in the present study.

SS concentrations are highly variable in arctic waters, and SS will contribute considerably more light attenuation in some arctic waterbodies than predicted by the model presented here. For example, in the Mackenzie River, when SS concentration reaches up to 150 g m^{-3}, CDOM contributes as little as 30% of UV light attenuation[20] and 10% of PAR attenuation;[76] the highest SS concentration has been reported to be around the magnitude of 1000 g m^{-3}.[77,78] Despite this, vertical mixing in large rivers like the Mackenzie is so strong that no mixing limitations are expected regardless of how much SS is present.

We found that 42% of the arctic lakes analyzed here exhibit partial or substantial limitation when they contain SS. This limitation is important because lakes account for most CO_2 emissions, including from photomineralization.[13] These findings demonstrate the need to better determine distributions of photochemical and hydrological parameters in arctic and other waters, to identify systems with mixing limitations and better estimate the effects. SS contributions to light attenuation in arctic waters are expected to increase, given that increased thermokarst activity and glacial melting associated with Arctic warming is expected to result in higher SS loads.[79,80] The photomineralization reaction efficiency model presented here can be used to assess the expected influence of hydrological and photochemical factors on photomineralization. For example, expected increases in summer precipitation[81,82] and enhanced thawing of the permafrost will increase discharge in arctic rivers. Increased discharge, which has been observed in Eurasian arctic rivers,[83] is often associated with increased concentrations of both SS and dissolved organic carbon in arctic rivers.[84] Increased discharge also generally corresponds to

increased water column depth in streams and rivers[85] (Fig. S4†). Both the dimensionless light attenuation and surface Damkohler number increase with water column depth, making mixing limitation more likely to occur. Enhanced permafrost thaw may lead to increased supply of labile CDOM,[10,86–88] although this may be counterbalanced by dilution due to higher discharge. Expected increase in cloud cover in the Arctic, due to warmer temperature and reduced sea ice cover,[89,90] will diminish light reaching the water surface, thereby reducing the primary driver of photomineralization, and correspondingly reducing the importance of mixing as a limiting factor.

Our numerical model quantifies mixing limitations for waterbodies where light decay is exponential over depth. Mixing limitation under other light decay profiles can be assessed qualitatively using this model. Mixing limitation becomes more pronounced when light attenuation is controlled by constituents other than CDOM, and when the CDOM distribution is more heterogeneous. Quantifying mixing limitation for waterbodies with non-exponential light profiles will require spatially explicit models that fully couple the distributions of light, CDOM, and SS over depth in the water column. Additional field data will be needed to assess the effects of SS for a wider range of Arctic systems, particularly to obtain site-specific light attenuation coefficients for SS and CDOM. Detailed understanding of spatial and temporal variability, such as how photolability of CDOM changes over time and how CDOM and SS inputs are distributed with space and time, will also improve prediction of photomineralization.

The present work is the first attempt to assess the effects of vertical hydrodynamic mixing on CDOM photomineralization rates. The study bridges hydrology and photochemistry, both of which are important controls on carbon dynamics, but are often studied separately. Our conceptual model identified the need to consider the effects of vertical mixing when CDOM is not the only light attenuating constituent. Our numerical model quantified effects of vertical mixing on photomineralization of DOC in arctic freshwaters where light decay over depth can be approximated as exponential. Mixing limitation is pronounced when light attenuation over depth is strong and when the photomineralization rate at the water surface exceeds the rate of CDOM replenishment from bottom waters. Relatively high mixing rates and low SS concentrations in most arctic waters mean that well-mixed assumptions used in prior work are valid in many, but not all, of these systems. This study improves our understanding and estimation of photomineralization rates in a warming arctic, which is critical for predicting how the arctic carbon cycle will respond to (and potentially amplify) climate change. This approach can be extended for other kinds of photochemical reactions in the water column, such as photochemical production of reactive oxygen species that are harmful to microorganisms,[58] photochemical production of ammonium or CO,[91] and photochemical alteration of DOC that influences microbial respiration.[9,13]

Conflicts of interest

There are no conflicts to declare.

Acknowledgements

This research was funded by National Science Foundation (NSF) grants ARC-1204220, CAREER-1351745, DEB-1026843, DEB-1637459, EAR-1344280, EAR-1351625, EAR-1417264, OPP-1022876, OPP-1023270, OPP-1107593, OPP-1504006, and by Institute of Sustainability and Energy at Northwestern (ISEN) Cluster fellowship. We thank K. H. Harrold and J. Dobkowski for help in the field. We thank Dr Mary Silber and her students for help with development of the theory underlying the model. This research was supported in part through the computational resources and staff contributions provided for the Quest high performance computing facility at Northwestern University, which is jointly supported by the Office of the Provost, the Office for Research, and Northwestern University Information Technology.

References

1 P. A. Raymond, J. Hartmann, R. Lauerwald, S. Sobek, C. McDonald, M. Hoover, D. Butman, R. Striegl, E. Mayorga, C. Humborg, P. Kortelainen, H. Duerr, M. Meybeck, P. Ciais and P. Guth, Global carbon dioxide emissions from inland waters, *Nature*, 2013, **503**, 355–359.
2 G. W. Kling, G. W. Kipphut and M. C. Miller, Arctic lakes and streams as gas conduits to the atmosphere: implications for tundra carbon budgets, *Science*, 1991, **251**, 298–301.
3 J. J. Cole, N. F. Caraco, G. W. Kling and T. K. Kratz, Carbon dioxide supersaturation in the surface waters of lakes, *Science*, 1994, **265**, 1568–1570.
4 P. A. Raymond, J. W. McClelland, R. M. Holmes, A. V. Zhulidov, K. Mull, B. J. Peterson, R. G. Striegl, G. R. Aiken and T. Y. Gurtovaya, Flux and age of dissolved organic carbon exported to the Arctic Ocean: A carbon isotopic study of the five largest arctic rivers, *Global Biogeochem. Cycles*, 2007, **21**(4), GB4011.
5 A. D. McGuire, L. G. Anderson, T. R. Christensen, S. Dallimore, L. Guo, D. J. Hayes, M. Heimann, T. D. Lorenson, R. W. Macdonald and N. Roulet, Sensitivity of the carbon cycle in the Arctic to climate change, *Ecol. Monogr.*, 2009, **79**, 523–555.
6 R. M. Holmes, J. W. McClelland, B. J. Peterson, S. E. Tank, E. Bulygina, T. I. Eglinton, V. V. Gordeev, T. Y. Gurtovaya, P. A. Raymond, D. J. Repeta, R. Staples, R. G. Striegl, A. V. Zhulidov and S. A. Zimov, Seasonal and annual fluxes of nutrients and organic matter from large rivers to the Arctic Ocean and surrounding seas, *Estuaries Coasts*, 2012, **35**, 369–382.
7 D. W. Kicklighter, D. J. Hayes, J. W. McClelland, B. J. Peterson, A. D. McGuire and J. M. Melillo, Insights and issues with simulating terrestrial DOC loading of Arctic river networks, *Ecol. Appl.*, 2013, **23**, 1817–1836.
8 R. G. Wetzel, P. G. Hatcher and T. S. Bianchi, Natural photolysis by ultraviolet irradiance of recalcitrant dissolved organic matter to simple substrates for rapid bacterial metabolism, *Limnol. Oceanogr.*, 1995, **40**, 1369–1380.

9 R. M. Cory, B. C. Crump, J. A. Dobkowski and G. W. Kling, Surface exposure to sunlight stimulates CO_2 release from permafrost soil carbon in the Arctic, *Proc. Natl. Acad. Sci. U. S. A.*, 2013, **110**, 3429–3434.
10 C. P. Ward and R. M. Cory, Complete and partial photo-oxidation of dissolved organic matter draining permafrost soils, *Environ. Sci. Technol.*, 2016, **50**, 3545–3553.
11 C. P. Ward, S. G. Nalven, B. C. Crump, G. W. Kling and R. M. Cory, Photochemical alteration of organic carbon draining permafrost soils shifts microbial metabolic pathways and stimulates respiration, *Nat. Commun.*, 2017, **8**, 772.
12 A. Stubbins, P. J. Mann, L. Powers, T. B. Bittar, T. Dittmar, C. P. McIntyre, T. I. Eglinton, N. Zimov and R. G. Spencer, Low photolability of yedoma permafrost dissolved organic carbon, *J. Geophys. Res.: Biogeosci.*, 2017, **122**, 200–211.
13 R. M. Cory, C. P. Ward, B. C. Crump and G. W. Kling, Sunlight controls water column processing of carbon in arctic fresh waters, *Science*, 2014, **345**, 925–928.
14 R. M. Cory, K. H. Harrold, B. T. Neilson and G. W. Kling, Controls on dissolved organic matter (DOM) degradation in a headwater stream: the influence of photochemical and hydrological conditions in determining light-limitation or substrate-limitation of photo-degradation, *Biogeosciences*, 2015, **12**, 6669–6685.
15 B. Koehler, T. Landelius, G. A. Weyhenmeyer, N. Machida and L. J. Tranvik, Sunlight-induced carbon dioxide emissions from inland waters, *Global Biogeochem. Cycles*, 2014, **28**, 696–711.
16 I. Laurion and N. Mladenov, Dissolved organic matter photolysis in Canadian arctic thaw ponds, *Environ. Res. Lett.*, 2013, **8**(3), 035026.
17 I. Laurion, W. F. Vincent and D. R. Lean, Underwater ultraviolet radiation: development of spectral models for northern high latitude lakes, *Photochem. Photobiol.*, 1997, **65**, 107–114.
18 S. Watanabe, I. Laurion, K. Chokmani, R. Pienitz and W. F. Vincent, Optical diversity of thaw ponds in discontinuous permafrost: A model system for water color analysis, *J. Geophys. Res.: Biogeosci.*, 2011, **116**(G2), G02003.
19 J. A. Gareis, L. F. Lesack and M. L. Bothwell, Attenuation of *in situ* UV radiation in Mackenzie Delta lakes with varying dissolved organic matter compositions, *Water Resour. Res.*, 2010, **46**(9), W09516.
20 L. Retamal, S. Bonilla and W. F. Vincent, Optical gradients and phytoplankton production in the Mackenzie River and the coastal Beaufort Sea, *Polar Biol.*, 2008, **31**, 363–379.
21 W. F. Vincent and J. Laybourn-Parry, *Polar lakes and rivers: limnology of Arctic and Antarctic aquatic ecosystems*, Oxford University Press, 2008.
22 P. B. Hamilton, K. Gajewski, D. E. Atkinson and D. R. Lean, Physical and chemical limnology of 204 lakes from the Canadian Arctic Archipelago, *Hydrobiologia*, 2001, **457**, 133–148.
23 W. F. Vincent and J. E. Hobbie, Ecology of Arctic lakes and rivers, *Arctic*, 2000, 197–231.
24 M. M. Squires and L. F. Lesack, Spatial and temporal patterns of light attenuation among lakes of the Mackenzie Delta, *Freshwater Biol.*, 2003, **48**, 1–20.
25 A. M. Milner and M. W. Oswood, *Freshwaters of Alaska: ecological syntheses*, Springer Science & Business Media, 2012.
26 M. E. Sierszen, M. E. McDonald and D. A. Jensen, Benthos as the basis for arctic lake food webs, *Aquat. Ecol.*, 2003, **37**, 437–445.
27 P. J. Neale, E. W. Helbling and H. E. Zagarese, Modulation of UVR exposure and effects by vertical mixing and advection, *UV effects in aquatic organisms ecosystems*, 2003, pp. 107–134.
28 R. F. Whitehead, S. De Mora, S. Demers, M. Gosselin, P. Monfort and B. Mostajir, Interactions of ultraviolet-B radiation, mixing, and biological activity on photobleaching of natural chromophoric dissolved organic matter: A mesocosm study, *Limnol. Oceanogr.*, 2000, **45**, 278–291.
29 C. M. Hu, F. E. Muller-Karger and R. G. Zepp, Absorbance, absorption coefficient, and apparent quantum yield: A comment on common ambiguity in the use of these optical concepts, *Limnol. Oceanogr.*, 2002, **47**, 1261–1267.
30 W. L. Miller, in *Aquatic humic substances*, Springer, 1998, pp. 125–143.
31 S. W. Zison, *Rates, constants, and kinetics formulations in surface water quality modeling*, Environmental Protection Agency, Environmental Research Laboratory, Athens, GA, 1978.
32 G. E. Likens, *Biogeochemistry of inland waters*, Academic Press, San Diego, CA, 2010.
33 S. C. Chapra, *Surface water-quality modeling*, Waveland press, Long Grove, IL, 2008.
34 D. Vachon, J.-F. Lapierre and P. A. del Giorgio, Seasonality of photochemical dissolved organic carbon mineralization and its relative contribution to pelagic CO_2 production in northern lakes, *J. Geophys. Res.: Biogeosci.*, 2016, **121**, 864–878.
35 M. Futter, D. Butterfield, B. Cosby, P. Dillon, A. Wade and P. Whitehead, Modeling the mechanisms that control in-stream dissolved organic carbon dynamics in upland and forested catchments, *Water Resour. Res.*, 2007, **43**(2), W02424.
36 M. P. Miller, D. M. McKnight, S. C. Chapra and M. W. Williams, A model of degradation and production of three pools of dissolved organic matter in an alpine lake, *Limnol. Oceanogr.*, 2009, **54**, 2213.
37 H. L. MacIntyre, T. M. Kana and R. J. Geider, The effect of water motion on short-term rates of photosynthesis by marine phytoplankton, *Trends Plant Sci.*, 2000, **5**, 12–17.
38 J. D. J. Ingle and S. R. Crouch, *Spectrochemical analysis*, 1988.
39 J. E. Hobbie, Carbon 14 measurements of primary production in two arctic Alaskan lakes: With 3 figures and 1 table in the text and on 1 folder, *Int. Ver. Theor. Angew. Limnol., Verh.*, 1964, **15**, 360–364.
40 R. Sommaruga, When glaciers and ice sheets melt: consequences for planktonic organisms, *J. Plankton Res.*, 2015, **37**, 509–518.

41 J. P. McNamara, D. L. Kane and L. D. Hinzman, An analysis of streamflow hydrology in the Kuparuk River basin, Arctic Alaska: A nested watershed approach, *J. Hydrol.*, 1998, **206**, 39–57.
42 D. L. Kane, J. P. McNamara, D. Q. Yang, P. Q. Olsson and R. E. Gieck, An extreme rainfall/runoff event in Arctic Alaska, *J. Hydrometeorol.*, 2003, **4**, 1220–1228.
43 B. J. Peterson, J. E. Hobbie, T. L. Corliss and K. Kriet, A continuous-flow periphyton bioassay: Tests of nutrient limitation in a tundra stream, *Limnol. Oceanogr.*, 1983, **28**, 583–591.
44 B. J. Peterson, J. E. Hobbie and T. L. Corliss, Carbon flow in a tundra stream ecosystem, *Can. J. Fish. Aquat. Sci.*, 1986, **43**, 1259–1270.
45 T. E. Osterkamp and M. W. Payne, Estimates of permafrost thickness from well logs in northern Alaska, *Cold Reg. Sci. Technol.*, 1981, **5**, 13–27.
46 A. Townsend-Small, J. W. McClelland, R. M. Holmes and B. J. Peterson, Seasonal and hydrologic drivers of dissolved organic matter and nutrients in the upper Kuparuk River, Alaskan Arctic, *Biogeochemistry*, 2011, **103**, 109–124.
47 T. V. King, B. T. Neilson, L. D. Overbeck and D. L. Kane, Water temperature controls in low arctic rivers, *Water Resour. Res.*, 2016, **52**, 4358–4376.
48 M. Nolan, Distribution of a Star3i DEM of the Kuparuk River watershed, Joint Office for Scientific Support, Boulder, Colorado, 2003, CD-ROM.
49 R. M. Cory, T. W. Davis, G. J. Dick, T. Johengen, V. J. Denef, M. A. Berry, S. E. Page, S. B. Watson, K. Yuhas and G. W. Kling, Seasonal dynamics in dissolved organic matter, hydrogen peroxide, and cyanobacterial blooms in Lake Erie, *Front. Mar. Sci.*, 2016, **3**, 54.
50 V. Katalin, B. Németh and L. Vörös, Specific attenuation coefficients of optically active substances and their contribution to the underwater ultraviolet and visible light climate in shallow lakes and ponds, *Hydrobiologia*, 2009, **632**, 91–105.
51 G. C. Miller and R. G. Zepp, Effects of suspended sediments on photolysis rates of dissolved pollutants, *Water Res.*, 1979, **13**, 453–459.
52 J. T. Kirk, *Light and photosynthesis in aquatic ecosystems*, Cambridge University Press, 1994.
53 S. MacIntyre, J. P. Fram, P. J. Kushner, N. D. Bettez, W. O'brien, J. Hobbie and G. W. Kling, Climate-related variations in mixing dynamics in an Alaskan arctic lake, *Limnol. Oceanogr.*, 2009, **54**, 2401–2417.
54 M. F. Merck and B. T. Neilson, Modelling in-pool temperature variability in a beaded arctic stream, *Hydrol. Processes*, 2012, **26**, 3921–3933.
55 K. M. Hinkel, J. D. Lenters, Y. Sheng, E. A. Lyons, R. A. Beck, W. R. Eisner, E. F. Maurer, J. Wang and B. L. Potter, Thermokarst lakes on the Arctic Coastal Plain of Alaska: Spatial and temporal variability in summer water temperature, *Permafr. Periglac. Process.*, 2012, **23**, 207–217.
56 L. A. Molot, J. J. Hudson, P. J. Dillon and S. A. Miller, Effect of pH on photo-oxidation of dissolved organic carbon by hydroxyl radicals in a coloured, softwater stream, *Aquat. Sci.*, 2005, **67**, 189–195.
57 P. Porcal, P. J. Dillon and L. A. Molot, Temperature dependence of photodegradation of dissolved organic matter to dissolved inorganic carbon and particulate organic carbon, *PLoS One*, 2015, **10**, e0128884.
58 S. E. Page, J. R. Logan, R. M. Cory and K. McNeill, Evidence for dissolved organic matter as the primary source and sink of photochemically produced hydroxyl radical in arctic surface waters, *Environ. Sci.: Processes Impacts*, 2014, **16**, 807–822.
59 S. Bertilsson and B. Allard, Sequential photochemical and microbial degradation of refractory dissolved organic matter in a humic freshwater system, *Arch. Hydrobiol.*, 1996, **48**, 133–141.
60 R. L. Panton, *Incompressible flow*, John Wiley & Sons, Hoboken, NJ, 4th edn, 2013.
61 D. Bolster, R. E. Hershberger and R. J. Donnelly, Dynamic similarity, the dimensionless science, *Phys. Today*, 2011, **64**, 42–47.
62 H. S. Fogler, *Elements of chemical reaction engineering*, Prentice Hall, Upper Saddle River, NJ, 4th edn, 2005.
63 M. M. Clark, *Transport modeling for environmental engineers and scientists*, John Wiley & Sons, San Diego, CA, 2nd edn, 2009.
64 M. Shapiro and H. Brenner, Dispersion of a chemically reactive solute in a spatially periodic model of a porous medium, *Chem. Eng. Sci.*, 1988, **43**, 551–571.
65 B. B. Dykaar and P. K. Kitanidis, Macrotransport of a biologically reacting solute through porous media, *Water Resour. Res.*, 1996, **32**, 307–320.
66 R. Aris, *The mathematical theory of diffusion and reaction in permeable catalysts*, Oxford Clarendon Press, Oxford, U.K., 1975.
67 J. E. Bailey and D. F. Ollis, *Biochemical engineering fundamentals*, McGraw-Hill Inc., USA, 1976.
68 S. Mishra, *Assigning probability distributions to input parameters of performance assessment models*, Swedish Nuclear Fuel and Waste Management Co., 2002.
69 J. Hammonds, F. Hoffman and S. Bartell, *An introductory guide to uncertainty analysis in environmental and health risk assessment*, US DOE, 1994.
70 B. J. Brewer, *1 Bayesian Inference and Computation: A Beginner's Guide, Bayesian Astrophysics*, 2018, vol. 26, p. 1.
71 M. Merck, B. Neilson, R. Cory and G. Kling, Variability of in-stream and riparian storage in a beaded arctic stream, *Hydrol. Processes*, 2012, **26**, 2938–2950.
72 B. Koehler, T. Landelius, G. A. Weyhenmeyer, N. Machida and L. J. Tranvik, Sunlight-induced carbon dioxide emissions from inland waters, *Global Biogeochem. Cycles*, 2014, **28**, 696–711.
73 B. Boehrer and M. Schultze, Stratification of lakes, *Rev. Geophys.*, 2008, **46**(2), RG2005.
74 H. B. Fischer, J. E. List, C. R. Koh, J. Imberger and N. H. Brooks, *Mixing in inland and coastal waters*, Elsevier, 2013.

75 S. Caplanne and I. Laurion, Effect of chromophoric dissolved organic matter on epilimnetic stratification in lakes, *Aquat. Sci.*, 2008, **70**, 123–133.

76 D. Doxaran, J. Ehn, S. Bélanger, A. Matsuoka, S. Hooker and M. Babin, Optical characterisation of suspended particles in the Mackenzie River plume (Canadian Arctic Ocean) and implications for ocean colour remote sensing, *Biogeosciences*, 2012, 3213–3229.

77 M. Carson, J. Jasper and F. M. Conly, Magnitude and sources of sediment input to the Mackenzie Delta, Northwest Territories, 1974–94, *Arctic*, 1998, 116–124.

78 J. A. Gareis and L. F. Lesack, Fluxes of particulates and nutrients during hydrologically defined seasonal periods in an ice-affected great Arctic river, the Mackenzie, *Water Resour. Res.*, 2017, **53**, 6109–6132.

79 B. Mindl, A. M. Anesio, K. Meirer, A. J. Hodson, J. Laybourn-Parry, R. Sommaruga and B. Sattler, Factors influencing bacterial dynamics along a transect from supraglacial runoff to proglacial lakes of a high Arctic glacieri, *FEMS Microbiol. Ecol.*, 2007, **59**, 307–317.

80 M. Jolivel and M. Allard, Impact of permafrost thaw on the turbidity regime of a subarctic river: the Sheldrake River, Nunavik, Quebec, *Arct. Sci.*, 2017, **3**, 451–474.

81 A. V. Pavlov, Current changes of climate and permafrost in the arctic and sub-arctic of Russia, *Permafr. Periglac. Process.*, 1994, **5**, 101–110.

82 R. A. Segal, T. C. Lantz and S. V. Kokelj, Acceleration of thaw slump activity in glaciated landscapes of the Western Canadian Arctic, *Environ. Res. Lett.*, 2016, **11**(3), 034025.

83 S. B. Rood, S. Kaluthota, L. J. Philipsen, N. J. Rood and K. P. Zanewich, Increasing discharge from the Mackenzie river system to the Arctic Ocean, *Hydrol. Processes*, 2016, **31**(1), 150–160.

84 J. W. McClelland, A. Townsend-Small, R. M. Holmes, F. Pan, M. Stieglitz, M. Khosh and B. J. Peterson, River export of nutrients and organic matter from the North Slope of Alaska to the Beaufort Sea, *Water Resour. Res.*, 2014, **50**, 1823–1839.

85 C. B. Phillips, *The control of grain-scale mechanics on channel form, landscape dynamics, and climatic perturbations in gravel-bedded rivers*, 2014.

86 B. W. Abbott, J. R. Larouche, J. B. Jones Jr, W. B. Bowden and A. W. Balser, Elevated dissolved organic carbon biodegradability from thawing and collapsing permafrost, *J. Geophys. Res.: Biogeosci.*, 2014, **119**, 2049–2063.

87 J. E. Vonk, P. J. Mann, S. Davydov, A. Davydova, R. G. M. Spencer, J. Schade, W. V. Sobczak, N. Zimov, S. Zimov, E. Bulygina, T. I. Eglinton and R. M. Holmes, High biolability of ancient permafrost carbon upon thaw, *Geophys. Res. Lett.*, 2013, **40**, 2689–2693.

88 J. E. Vonk, S. E. Tank, W. B. Bowden, I. Laurion, W. F. Vincent, P. Alekseychik, M. Amyot, M. F. Billet, J. Canario, R. M. Cory, B. N. Deshpande, M. Helbig, M. Jammet, J. Karlsson, J. Larouche, G. MacMillan, M. Rautio, K. M. W. Anthony and K. P. Wickland, Reviews and syntheses: Effects of permafrost thaw on Arctic aquatic ecosystems, *Biogeosciences*, 2015, **12**, 7129–7167.

89 N. P. Barton and D. E. Veron, Response of clouds and surface energy fluxes to changes in sea-ice cover over the Laptev Sea (Arctic Ocean), *Clim. Res.*, 2012, **54**, 69–84.

90 G. H. F. Young, D. McCarroll, N. J. Loader, M. H. Gagen, A. J. Kirchhefer and J. C. Demmler, Changes in atmospheric circulation and the Arctic Oscillation preserved within a millennial length reconstruction of summer cloud cover from northern Fennoscandia, *Clim. Dyn.*, 2012, **39**, 495–507.

91 M. A. Moran and R. G. Zepp, Invited Review Role of photoreactions in the formation of biologically labile compounds from dissolved organic matter, *Oceanography*, 1997, **42**(6), 1307–1316.

